

# The Magnification Invariant of Circularly-symmetric Lens Models

Chengliang Wei<sup>1,2</sup>, Zhe Chu<sup>1,3</sup> and Yiping Shu<sup>1,3</sup>

<sup>1</sup> Purple Mountain Observatory, the Partner Group of MPI für Astronomie, 8 Yuanhua Road, Nanjing 210033, China; *chengliangwei@pmo.ac.cn*

<sup>2</sup> University of Chinese Academy of Science, 19A Yuquan Road, 100049 Beijing, China

<sup>3</sup> School of Astronomy and Space Sciences, University of Science and Technology of China, 230029 Hefei, China

**Abstract** In the context of strong gravitational lensing, the magnification of image is of crucial importance to constrain various lens models. For several commonly used quadruple lens models, the magnification invariants, defined as the sum of the signed magnifications of images, have been analytically derived when the image multiplicity is a maximum. In this paper, we further study the magnification of several disk lens models, including (a) exponential disk lens, (b) Gaussian disk lens, (c) modified Hubble profile lens, and another two of the popular three-dimensional symmetrical lens model, (d) NFW lens and (e) Einasto lens. We find that magnification invariant does also exist for each lens model. Moreover, our results show that magnification invariants can be significantly changed by the characteristic surface mass density  $\kappa_c$ .

**Key words:** Gravitational lensing: strong – Methods: numerical

## 1 INTRODUCTION

As one of the promising ways to explore cosmological information, strong gravitational lensing has been investigated in many astrophysical studies (e.g., [Paraficz 2009](#); [Cao et al. 2015](#); [McKean et al. 2015](#); [Yuan & Wang 2015](#)): for determining the mass density profile of galaxies (e.g., [Koopmans et al. 2009](#); [Vegetti et al. 2012](#); [Shu et al. 2016, 2017](#)), measuring the masses of central black holes in distant quiescent galaxies (e.g., [Mao et al. 2001](#); [Rusin et al. 2005](#)), and estimating Hubble constant using time delays between multiple images in the observed lensing systems (e.g., [Biggs et al. 1999](#); [Fassnacht et al. 2002](#); [Tortora 2007](#); [Linder 2011](#); [Suyu et al. 2014](#)).

In the context of strong gravitational lensing, multiple images of a given background source can be produced when the lensing system has a well alignment between the observer, the lens, and the source ([Burke 1981](#); [Dyer & Roeder 1980](#); [Meylan et al. 2006](#)). Based on the magnification theorem, the total image number of a lens is odd if the lens has a smooth surface mass density. On the other hand, the gravitational

Table 1: Magnification invariants for some four-image lens models<sup>a</sup>.

Lens model	Lens potential $\psi$	$I^b (= \sum_i \mu_i)$
1. SIED( $x, y$ )	$x\alpha_x + y\alpha_y$	$\approx 2.8$
2. SIEP( $x, y$ )	$b\sqrt{q^2x^2 + y^2}$	2
3. SIQ( $\theta, \phi$ )	$\theta_E\theta - \frac{1}{3}\theta_E k\theta \cos 2\phi$	1
4. SIS+shear( $\theta, \phi$ )	$\theta_E\theta - \frac{\gamma}{2}\theta^2 \cos 2\phi$	$2/(1 - \gamma^2)$
5. point+shear( $\theta, \phi$ )	$\theta_E^2 \ln \theta - \frac{\gamma}{2}\theta^2 \cos 2\phi$	$1/(1 - \gamma^2)$

Notes. <sup>a</sup> Here  $b$  is a constant parameter,  $q$  is the axial ratio in the SIEP lens,  $\theta_E$  is the Einstein radius,  $k(0 \leq k \leq 1)$  is the intensity of the quadrupole relative to the monopole in the SIQ lens, and  $\gamma$  indicates the external shear [Chu et al. \(2015\)](#). <sup>b</sup> [Dalal \(1998\)](#); [Dalal & Rabin \(2001\)](#); [Witt & Mao \(2000\)](#)

lensing is able to magnify the apparent brightness of the source ([Schneider et al. 1992](#)). Thus the connection between magnification and multiple images is crucial in a variety of studies of gravitational lensing ([Witt & Mao 2000](#); [Aazami & Petters 2009](#); [Werner 2009](#); [Petters & Werner 2010](#); [Tsukamoto & Harada 2013](#); [Chu et al. 2015](#)). For example, the summation of the image magnification for a point lens and singular isothermal sphere (SIS) lens is 1 and 2 respectively, regardless of the source positions and how large the Einstein radii are. In [Dalal \(1998\)](#), the author found that the summation of signed magnifications of all the images ( $I = \sum_i \mu_i$ , where  $\mu_i$  denotes the signed magnification of the  $i^{\text{th}}$  image) is a constant for several quadrupole lens models when the image number is a maximum. Conventionally, this constant ( $I$ ) is dubbed 'magnification invariant'. In [Chu et al. \(2015\)](#), they studied several lens models, including (1) singular isothermal elliptical density (SIED), (2) singular isothermal elliptical potential (SIEP), (3) singular isothermal quadrupole (SIQ), (4) SIS + external shear and (5) point + external shear lenses. The magnification invariants for these models are shown in Tab. 1. It is found that the invariant is independent of most of the model parameters, as long as the source lies inside of the caustic.

If the surface mass density of a lens is circularly symmetric, the lensing properties, such as deflection angle and lensing shear, can be derived analytically. While it is not clear whether a magnification invariant can be found in the circularly-symmetric lens system (hereafter circular lens). In this paper, we study the magnification invariant of the circular lens by considering several commonly used lens models, like exponential disk lens and Gaussian disk lens. Moreover, as found in the numerical  $N$ -body simulations, the density profile of a cold dark matter halo can be described by the NFW profile ([Navarro et al. 1997](#)). While recent high-resolution simulations show that Einasto radial profile, which is a non-singular three-parameter model, provides a more accurate description of dark matter haloes ([Elfasdóttir & Möller 2007](#); [Navarro et al. 2004, 2010](#)). For these two popular spherical symmetrical density profiles, we can derive their projected surface mass density by integrating the three-dimensional density profile along the line of sight. The investigation of the magnification invariant is important to constrain these lens models.

The rest of this paper is organized as follows. In Sec. 2, we briefly summarize the basics of circular lens, and several commonly used lens models. In Sec. 3, we describe our method to derive the magnification

invariants for each discussed lens model and show the dependency between derived invariants and lensing parameters. Conclusions and discussions are summarized in Sec. 4.

## 2 CIRCULAR LENS

An arbitrary surface mass density  $\Sigma(\boldsymbol{\theta})$  can be expanded in terms of a complete set of orthogonal basis functions (e.g., [Trotter et al. 2000](#)), which can decompose  $\Sigma(\boldsymbol{\theta})$  into multipole components,

$$\Sigma(\boldsymbol{\theta}) = \Sigma_0(\theta) + \sum_{m=1}^{\infty} [A_m(\theta) \cos(m\chi) + B_m(\theta) \sin(m\chi)], \quad (1)$$

where  $\theta$  is the distance from the lens centre,  $\chi$  is the polar angle. The first term  $\Sigma_0(\theta) = 1/2\pi \int_0^{2\pi} \Sigma(\boldsymbol{\theta}) d\chi$  is known as the monopole. The higher-order multipoles ( $m \geq 1$ ) represent the angular structure of the mass distribution, which are composed of two parts ( $A_m$  and  $B_m$ ). Because of the symmetry, circular lenses can be fully described by its monopole. As a kind of ideal lens model, most of properties can be given analytically for a given circular lens ([Miralda-Escude 1991](#); [Schneider et al. 1992](#); [Narayan & Bartelmann 1999](#)). In this section, we present the basics for our analysis, and also describe several commonly discussed circular lens models. Throughout the paper we denote the observed angular position on the lens plane by  $\boldsymbol{\theta} = \theta(\cos \chi, \sin \chi)$  and its source position by  $\boldsymbol{\beta}$ .

### 2.1 Basics of Circular Lens

In general, if the mass distribution of a lens object is circularly-symmetric, the 2D Poisson equation,  $\nabla^2 \psi(\boldsymbol{\theta}) = 2\kappa(\boldsymbol{\theta})$ , can be reduced to a function only of the distance from the lens centre  $\theta = |\boldsymbol{\theta}|$ ,

$$\frac{1}{\theta} \frac{\partial}{\partial \theta} \left( \theta \frac{\partial}{\partial \theta} \right) \psi(\theta) = 2\kappa(\theta), \quad (2)$$

where  $\psi(\theta)$  is the deflection potential, and  $\kappa(\theta) = \Sigma(\theta)/\Sigma_{\text{crit}}$  is the dimensionless surface mass density in unit of the critical surface mass density  $\Sigma_{\text{crit}} = c^2 D_s / 4\pi G D_d D_{ds}$ . Here  $D_d$ ,  $D_s$  and  $D_{ds}$  are the angular diameter distance to the lens, to the source and between the lens and the source, respectively. For circular lens, deflection angle  $\alpha(\theta)$ , lensing shear  $\gamma(\theta)$  and magnification  $\mu(\theta)$  are given as ([Miralda-Escude 1991](#); [Meylan et al. 2006](#)),

$$\alpha(\theta) = \theta \bar{\kappa}(\theta), \quad (3)$$

$$\gamma(\theta) = \bar{\kappa}(\theta) - \kappa(\theta) = \frac{\alpha(\theta)}{\theta} - \kappa(\theta), \quad (4)$$

$$\frac{1}{\mu(\theta)} = \left[ 1 - \frac{\alpha(\theta)}{\theta} \right] \left[ 1 + \frac{\alpha(\theta)}{\theta} - 2\kappa(\theta) \right]. \quad (5)$$

where  $\bar{\kappa}(\theta) = \bar{\Sigma}(\theta)/\Sigma_{\text{crit}}$  is the mean surface mass density inside  $\theta$ . Since the critical curves arise at  $1/\mu = 0$ , Eq. 5 implies that the circular lens has a pair of critical curves ([Meylan et al. 2006](#)). The one,  $1 - \alpha(\theta)/\theta = 0$ , is the tangential critical curve, which corresponds to the Einstein Ring with Einstein radius. The another,  $1 + \alpha(\theta)/\theta - 2\kappa(\theta) = 0$ , is called radial critical curve, which also defines a ring and the corresponding radius.

In the strong gravitational lensing, multiple images can be produced for a given source. The image number depends on the position of the source with respect to the caustics, which are the mapping of the critical curves in the source plane. For circular lenses, since the tangential critical curve does not lead to a

caustic curve and the corresponding caustic degenerates to a single point  $\beta = 0$ , the tangential critical curve has no influence on the image multiplicity. Thus, pairs of images can only be created or destroyed if the radial critical curve exists. When a source lies inside of the radial caustic, three images will be produced at most. In general, to derive the magnifications of the images, the lens equation should be solved numerically.

In the rest of this section, we will discuss several often used circular lens models, which can be analyzed analytically and are useful for theoretical investigations.

## 2.2 Circular Lens Models

The first lens model considered in this work is an exponential disk model, usually used to describe the mass distribution of a spiral galaxy (Lehár et al. 2000). For an exponential disk model with  $\Sigma(\theta) = \Sigma_0 \exp(-\theta/\theta_0)$ , the convergence can be obtained as

$$\kappa_E(\theta) = \kappa_0 \exp(-\theta/\theta_0). \quad (6)$$

where  $\kappa_0$  is the central dimensionless surface mass density and  $\theta_0$  is the scale length of the lens model. The scaled deflection angle  $\alpha(\theta)$  and lensing shear  $\gamma(\theta)$  are derived as shown in Tab. 2, and these lensing properties are shown in Fig. 1. Clearly, two critical curves can be identified, where  $\mu(\theta) = \infty$ , in the figure of the magnification (in the lower-right panel). Different colors indicate that lens plane can be divided into three image region by the two critical curves. The Fermat maximum image lies in the black line region around the centre of the lens, and it has a positive magnification. The minimum image arises in the blue line region, which is outskirts of the lensing disk, and its magnification is also positive. The saddle image can be found in red line region, which has the negative magnification, and here we flip the signs in the figure. In the left panel of Fig. 2, we show the distribution of the absolute value of the magnification in logarithm ( $\log |\mu|$ ) in the lens plane.

Based on the lens equation, the positions of images for a given source are calculated as

$$\beta = \theta - \frac{2\kappa_0}{\theta} [\theta_0^2 - \theta_0(\theta + \theta_0)\exp(-\theta/\theta_0)]. \quad (7)$$

Here, the image position  $\theta$  can not be solved analytically. Thereby, it is also difficult to derive the magnifications of the three images. In this work, we use of a precise numerical ray-tracing method, developed by Chu et al. (2016), to calculate the positions and corresponding magnifications of different images for a given source. The results can be found in section 3.

We also consider another two circular lens models: The dimensionless density profile is given as  $\kappa_G(\theta) = \kappa_0 \exp(-\theta^2/\theta_0^2)$ , dubbed as Gaussian disk lens. This model can be used to describe Einasto lens with index 1/2, as represented in Sec. 2.4. The other is the so-called modified Hubble profile (Rood et al. 1972), and the projected surface mass density of this lens model is given as,

$$\Sigma(\theta) = \frac{\Sigma_0}{1 + \theta^2/\theta_0^2}, \quad (8)$$

which is a softened power law lens, and the dimensionless projected surface density can be expressed as  $\kappa_{MH}(\theta) = \kappa_0 \theta_0^2 / (\theta^2 + \theta_0^2)$ . For these two important lens models, their lensing properties ( $\alpha$ ,  $\gamma$ , and  $\mu$ ) are listed in Tab. 2, respectively.

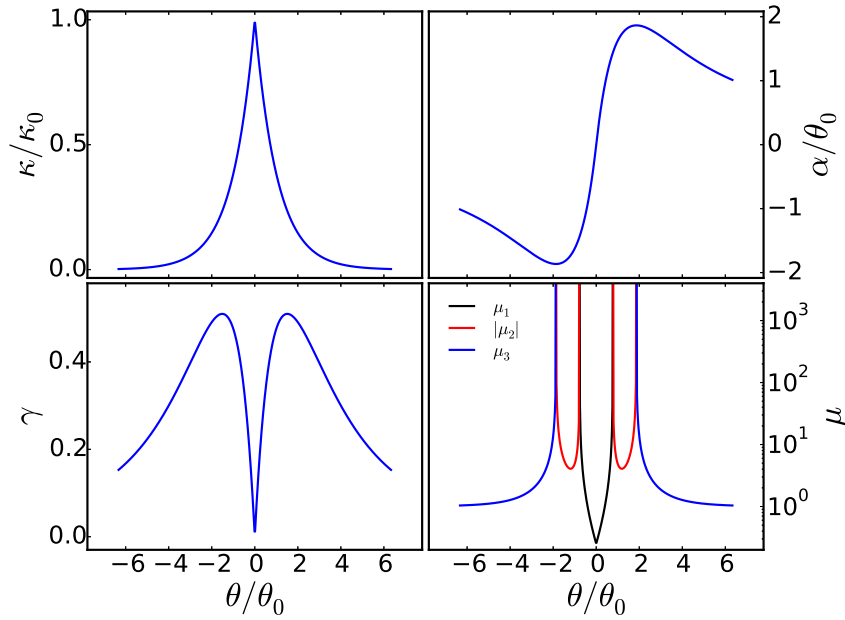


Fig. 1: The convergence  $\kappa(\theta)$ , deflection angle  $\alpha(\theta)$ , shear  $\gamma(\theta)$ , and magnification  $\mu(\theta)$  for a typical exponential disk lens.

Table 2: Lens properties of the three circular lens models.

Lens model	Convergence $\kappa(\theta)$	Deflection angle $\alpha(\theta)$	Shear $\gamma(\theta)$
1. Exponential disk	$\kappa_0 \exp(-\theta/\theta_0)$	$\frac{2\kappa_0}{\theta} [\theta_0^2 - \theta_0(\theta + \theta_0)\exp(-\theta/\theta_0)]$	$\frac{\kappa_0}{\theta^2} [2\theta_0^2 - (\theta^2 + 2\theta\theta_0 + 2\theta_0^2)\exp(-\theta/\theta_0)]$
2. Gaussian disk	$\kappa_0 \exp(-\theta^2/\theta_0^2)$	$\frac{\kappa_0 \theta_0^2}{\theta} [1 - \exp(-\theta^2/\theta_0^2)]$	$\frac{\kappa_0}{\theta^2} [\theta_0^2 - (\theta^2 + \theta_0^2)\exp(-\theta^2/\theta_0^2)]$
3. Modified Hubble profile	$\kappa_0 \theta_0^2 / (\theta^2 + \theta_0^2)$	$\frac{\kappa_0 \theta_0^2}{\theta} \ln(\theta^2/\theta_0^2 + 1)$	$\frac{\kappa_0 \theta_0^2}{\theta^2} \left[ \ln(\theta^2/\theta_0^2 + 1) - \frac{\theta^2}{\theta^2 + \theta_0^2} \right]$

### 2.3 NFW lens

As a typical model for describing the density distribution of dark matter halo, the NFW density profile is written as (Navarro et al. 1997; Wright & Brainerd 2000),

$$\rho(r) = \frac{\delta_c \rho_c}{(r/r_s)(1 + r/r_s)^2}, \quad (9)$$

where  $\rho_c$  is the critical density of the universe. The scale radius,  $r_s = r_{200}/c$ , is a characteristic radius of the halo, where  $c$  is the concentration parameter and the characteristic overdensity  $\delta_c$  for the halo is

$$\delta_c = \frac{200}{3} \frac{c^2}{\ln(1+c) - c/(1+c)}. \quad (10)$$

With the thin lens approximation, we define the line of sight as the optical axis  $z$ , and the three-dimensional NFW density profile  $\rho(D_d \boldsymbol{\theta}, z)$  will be reduced as two-dimensional surface mass density (e.g., Golse & Kneib 2002; Hurtado et al. 2014),

$$\Sigma(x) = \int_{-\infty}^{+\infty} \rho(x; z) dz = 2\Sigma_s F(x), \quad (11)$$

Here the dimensionless radial distance  $x = \theta/\theta_s$ , where  $\theta_s = r_s/D_d$ .  $\Sigma_s = \delta_c \rho_c r_s$  is defined as the characteristic surface mass density, and the factor  $F(x)$  is

$$F(x) = \begin{cases} \frac{1}{x^2-1} \left( 1 - \frac{1}{\sqrt{1-x^2}} \operatorname{arccosh} \frac{1}{x} \right) & (x < 1) \\ \frac{1}{3} & (x = 1) \\ \frac{1}{x^2-1} \left( 1 - \frac{1}{\sqrt{x^2-1}} \arccos \frac{1}{x} \right) & (x > 1) \end{cases}. \quad (12)$$

Additionally, the mean surface density inside the dimensionless radius  $x$  is

$$\bar{\Sigma}(x) = \frac{1}{\pi x^2} \int_0^x 2\pi x \Sigma(x) dx = 4\Sigma_s \frac{G(x)}{x^2}, \quad (13)$$

with

$$G(x) = \begin{cases} \ln \frac{x}{2} + \frac{1}{\sqrt{1-x^2}} \operatorname{arccch} \frac{1}{x} & (x < 1) \\ \ln \frac{1}{2} + 1 & (x = 1) \\ \ln \frac{x}{2} + \frac{1}{\sqrt{x^2-1}} \arccos \frac{1}{x} & (x > 1) \end{cases}. \quad (14)$$

Then the deflection angle  $\alpha$  between the source and the image, the convergence  $\kappa$  and the shear  $\gamma$  can be derived,

$$\begin{cases} \alpha(x) = 4\kappa_s \frac{G(x)}{x} \\ \kappa(x) = 2\kappa_s F(x) \\ \gamma(x) = \bar{\kappa}(x) - \kappa(x) = 2\kappa_s \left[ \frac{2G(x)}{x^2} - F(x) \right] \end{cases}. \quad (15)$$

As discussed in [Bartelmann \(1996\)](#), since  $(d\alpha/dx)$  is continuous, NFW lens can still produce three images at most, despite of its central singularity.

## 2.4 Einasto lens

Recent  $N$ -body simulations indicate that a non-singular three-parameter model such as the Einasto profile can provide a better description of dark matter haloes in a wide range of halo mass than the NFW profile (e.g., [Navarro et al. 2004, 2010](#); [Elíasdóttir & Möller 2007](#); [Dhar & Williams 2010](#); [Serenio et al. 2016](#)). The profile of an Einasto halo is ([Retana-Montenegro & Frutos-Alfaro 2011](#)),

$$\rho(r) = \rho_0 \exp \left[ - \left( \frac{r}{h} \right)^{1/n} \right], \quad (16)$$

where  $\rho_0$  is central density, and  $h$  is the scale length,  $n$  is the Einasto index. Clearly, the Einasto profile corresponding to  $n = 1$  is an exponential model in 3D, and  $n = 1/2$  gives a Gaussian model. With the thin lens approximation, the projected surface mass density of Einasto lens model is given by integrating along the line of sight of the 3D density profile as in Eq. 11,

$$\Sigma(x) = \int_{-\infty}^{+\infty} \rho(x; z) dz = 2 \int_x^{\infty} \frac{\rho(r) r dr}{\sqrt{r^2 - x^2}}, \quad (17)$$

where  $r = \sqrt{x^2 + z^2}$ , and we has rewritten the integration as Abel transform ([Binney & Tremaine 1987](#)) in the right term. As studied in [Retana-Montenegro et al. \(2012a,b\)](#), they derived the surface mass density of Einasto by a Mellin integral transform formalism, and related lensing properties in terms of the Fox  $H$  and Meijer  $G$  functions. More details can be referred to [Retana-Montenegro et al. \(2012b\)](#).

Table 3: The lensing functions  $\alpha(\theta)$ ,  $\kappa(\theta)$ , and  $\gamma(\theta)$  for Einasto model with  $n = 1$  and  $n = 1/2$ . Here  $\kappa_s$  is the central convergence, and  $x$  defines the dimensionless radius as  $x = \theta/\theta_s$ .  $K_\nu(x)$  is the modified Bessel function of the second kind of order  $\nu$ .

Einasto index $n$	Convergence $\kappa(x)$	Deflection angle $\alpha(x)$	Shear $\gamma(x)$
$n = 1$	$\kappa_s x K_1(x)$	$\frac{4\kappa_s}{x} \left[ 1 - \frac{x^2}{2} K_2(x) \right]$	$\frac{4\kappa_s}{x^2} \left[ 1 - \frac{x^2}{2} K_2(x) - \frac{x^3}{4} K_1(x) \right]$
$n = 1/2$	$\kappa_s \exp(-x^2)$	$\frac{\kappa_s}{x} [1 - \exp(-x^2)]$	$\frac{\kappa_s}{x^2} [1 - (1 + x^2) \exp(-x^2)]$

Here, as a comparison with the exponential disk lens and Gaussian disk lens model in 2D, we will present the lensing properties for the two often used models, exponential model and Gaussian model, in 3D. Using the specific Meijer  $G$  function, we can derive the surface mass density profile and lensing properties. Tab. 3 shows the lensing properties for the two considered models, and it is found that Einasto model with  $n = 1/2$  can be reduced to a Gaussian disk lens model.

### 3 MAGNIFICATION INVARIANTS

#### 3.1 The Test of Magnification Summation

With the purpose of calculating the accurate position of the image and its corresponding magnification for a given source, we utilize the analytical ray-tracing method in different image regions to numerically evaluate magnification for each image. This precise numerical method has been introduced in [Chu et al. \(2016\)](#) to study the magnification relations of quad lenses, which is shortly described as follows.

For a well-defined circular lens model, when the source lies in the radial caustic, one can find three images at most. Therefore, we pixelate the region in the radial caustic as the source area, so as to find images of it by the analytical deflection angles. As shown in Fig. 2, the image of the source area can be divided into three parts in the lens plane. Each point source in the source region has three corresponding images. The saddle image lies in image region 2 with negative magnification. The other two images, lying in image region 1 and 3, arise at the maxima and minima of the time delay surface, hence they have positive magnification.

For the sake of calculating the magnifications of the three images for a given point source  $\mathcal{P}$  inside of the caustic, we need to obtain the exact positions of the three images in the lens plane. At first, we set a bundle of light rays from the observer to grids in the image region 1, and then the deflected light rays will be traced back to the source region. Clearly, the image position of the source  $\mathcal{P}$  can be approximately estimated by the nearest light ray to the given point source. Starting from this approximate position of image, we are able to calculate the image positions accurately for each point source in the source region by using Newton-Raphson method.

After deriving the positions of the images and their magnifications  $\mu$  for the given lens model, we can map the divided image regions in right panel of Fig. 2 to the source plane, and estimate the magnification summation for each source. Using this numerical method, images can be matched to their source precisely in different image region.

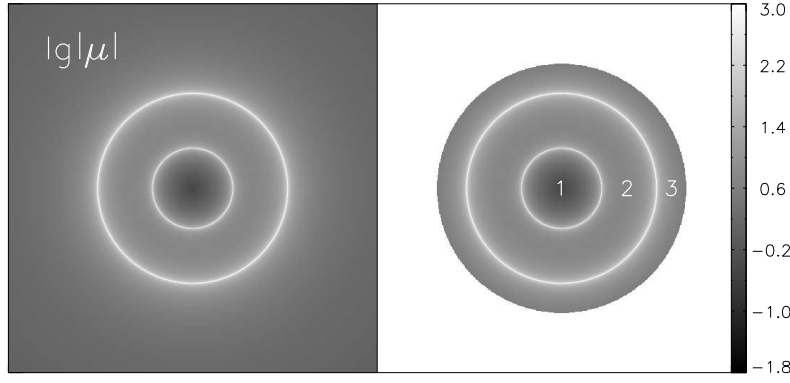


Fig. 2: The distribution of different image regions by a circularly-symmetric lens. The left panel shows the absolute value of the magnification  $\mu$  in logarithm. The right panel shows the three image regions corresponding to the source region inside of the caustic, where the gray values are derived from the left panel.

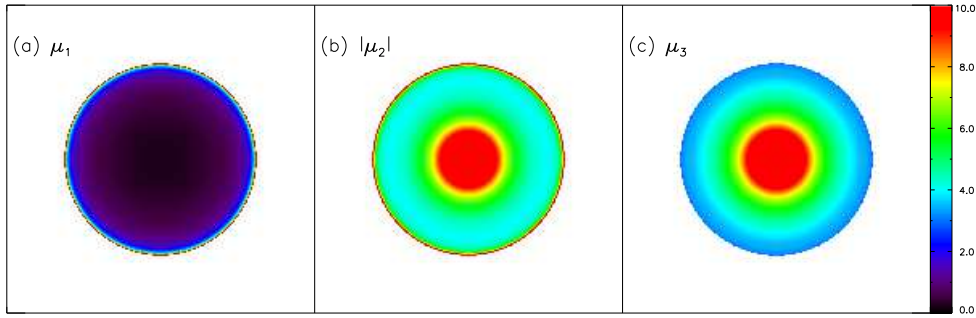


Fig. 3: The magnification distributions as functions of source positions. The values are mapped from three different image regions to source plane respectively. The left panel shows magnification  $\mu_1$  of the image region 1, which is corresponding to the maxima of the time delay surface. The middle panel presents images that arise at the saddle points of the time delay surface with the negative magnification  $\mu_2$ , so here we flipped the sign of the magnification. The magnification  $\mu_3$  of image region 3, which arises at the minima of the time delay surface, is shown in the right panel.

For the exponential disk lens, we have analytically derived the scaled deflection angle  $\alpha$  and the magnification  $\mu$  from the 2D Poisson equation in section 2.2. Employing the numerical method introduced above, we can map the magnifications of the three different regions in right panel of Fig. 2 into the source plane accurately, and the results are shown in Fig. 3. The left panel shows magnification  $\mu_1$  of the image region 1, which is corresponding to the maxima of the time delay surface, and generally demagnified. The middle panel presents images that arise at the saddle points of the time delay surface with the negative magnification  $\mu_2$ . Here we flipped the sign of the magnification. The magnification  $\mu_3$  of image region 3, which arises at the minima of the time delay surface, is shown in the right panel.

With these image magnification in different image region shown in Fig. 3, we calculate the magnification summation by  $\sum_i \mu_i = \mu_1 + \mu_2 + \mu_3$ , and the result is shown in the left panel of Fig. 4 by black dots. Here the source position  $\beta$  has been normalized by the radial caustic  $\beta_{\text{caus}}$ , and the error bars are estimated from



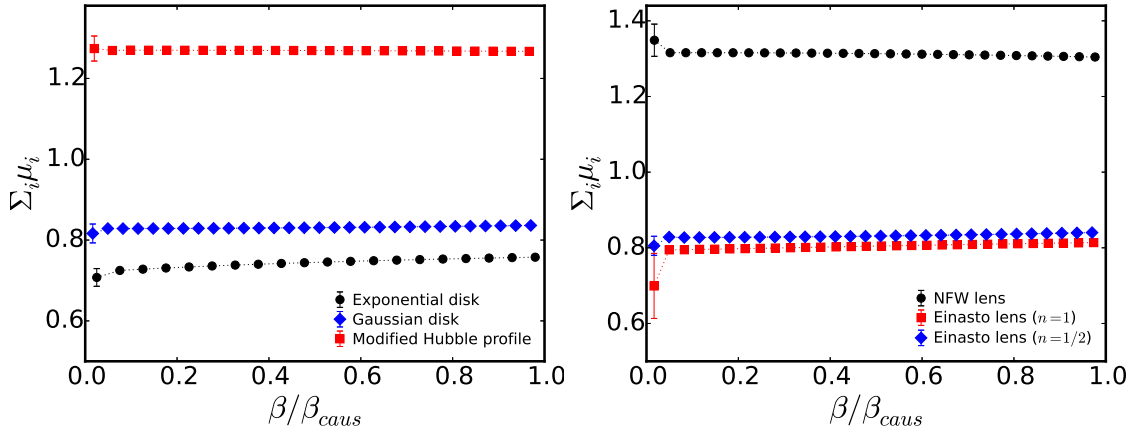


Fig. 4: The summation of signed magnifications of images for the given disk lens models in the left panel and the NFW/Einasto lens models in the right panel. Source positions are scaled by the radius of radial caustic,  $\beta_{caus}$ .

the different radial bins. Note that the large error around the center happens because of the magnification changes fast with the increasing of the radius. For arbitrary source positions within the caustic for a given set of  $\kappa_0$  and  $\theta_0$ , the summed magnification is almost constant, but with a subtle change, and can be evaluated by the mean value as  $0.75 \pm 0.03$  here.

Analogous to exponential disk lens model, we also calculate magnification summation for Gaussian model and modified Hubble profile lens model as shown in the left panel of Fig. 4, and in the right panel we show the magnification summations for the NFW lens and Einasto lens. We find the magnification summations are almost constant for these lens models, regardless of the position for the source in the radial caustic.

### 3.2 Dependence of Invariants on the Model Parameters

In general, for a two-parameter circular lens model, its dimensionless surface mass density can be generally defined by the characteristic surface mass density  $\kappa_c$  and the radial distribution function  $f(\theta/\theta_c)$ ,

$$\kappa(\theta) = \kappa_c f(\theta/\theta_c), \quad (18)$$

where  $\kappa_c$  can be  $\kappa_0$  in the disk lens model or  $\kappa_s$  in NFW and Einasto lens models,  $\theta_c$  is the characteristic radius of the lens model, such as  $\theta_0$  in exponential disk lens model and  $\theta_s$  in NFW and Einasto lens models. If a dimensionless radial distance  $x = \theta/\theta_c$  is defined in these circular lens models, we find the lensing properties will not be changed. Thus the magnification invariants should not depend on the characteristic radius  $\theta_c$ . For given model parameters  $(\kappa_c, \theta_c)$ , the magnification invariant can be numerically estimated as represented above. While the dependency between the invariant and the model parameters is unclear. In this section, we test how the magnification invariant depends on the models parameters  $\kappa_c$  and  $\theta_c$ .

We first verify the feasibility of our method for determining magnification invariant by considering the well defined lens model with the non-singular isothermal sphere, termed NIS (e.g., [Kormann et al. 1994](#); [Aubert et al. 2007](#)), which is an isothermal sphere with small but finite core,

$$\kappa_{NIS}(\theta) = \frac{\kappa_c}{2\sqrt{\theta^2/\theta_c^2 + 1}}. \quad (19)$$

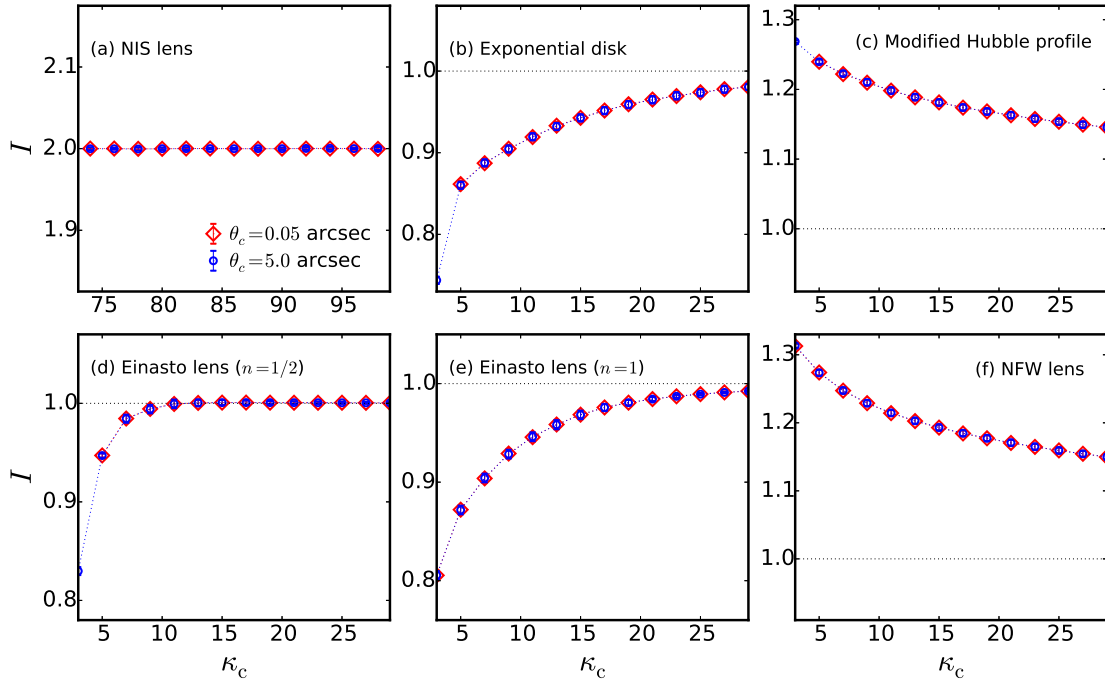


Fig. 5: The magnification invariants with the different model parameters  $\kappa_c$  and  $\theta_c$ . NIS model shows a constant magnification invariant, which is independent of model parameters. While, for the other lens models, the characteristic surface mass density  $\kappa_c$  can change the invariants significantly.

For this specific model of the circular lens, one can analytically calculate the magnification summation of the three images. In Appendix A, we theoretically prove that the magnification invariant of NIS equals 2, which is a constant without dependence of models parameters  $\kappa_c$  and  $\theta_c$ . As a comparison, we estimate the magnification invariant  $I$  through our numerical method for the NIS model. The invariants are evaluated by the mean value of the magnification summation  $\sum_{i=1}^3 \mu_i$  at different source position, as the function of different model parameters,  $\kappa_c$  and  $\theta_c$ . Fig. 5(a) shows the magnification invariants with different parameters for NIS model. Clearly, our numerical result indicates that the invariant of NIS lens is equal to 2, and this magnification invariant is independent of model parameters, which agrees well with the prediction in Appendix A.

Using our numerical method, we investigate magnification invariants for the given lens models, and show the results in Fig. 5. We find that the invariants do not change for different scale length  $\theta_c$  as we expected. But the characteristic surface mass density  $\kappa_c$  can change the invariants significantly. When  $\kappa_c$  is large enough, the magnification invariants converge to 1 for both exponential disk lens and Einasto lens. Note that for Einasto model the index  $n$  is very important in determining the surface mass density characteristics, which determine the lensing properties of the respective profiles. Thus with different index  $n$ , the converged value of magnification invariants may be different. Moreover, the invariants of exponential disk lens and Einasto lens (both  $n = 1/2$  and 1) increase monotonically over the characteristic surface mass density  $\kappa_c$ , while decrease for the modified Hubble profile and NFW lens.

This difference should be resulted by the different density profiles of the lens models. Fig. 6 shows the density profile of the used lens models in this paper. Clearly, for the exponential disk lens and Einasto lens (both  $n = 1/2$  and 1), their density profiles remarkably decrease to  $\lesssim 10^{-2} \kappa_c$  at  $\theta \sim 5\theta_c$ . While for NFW

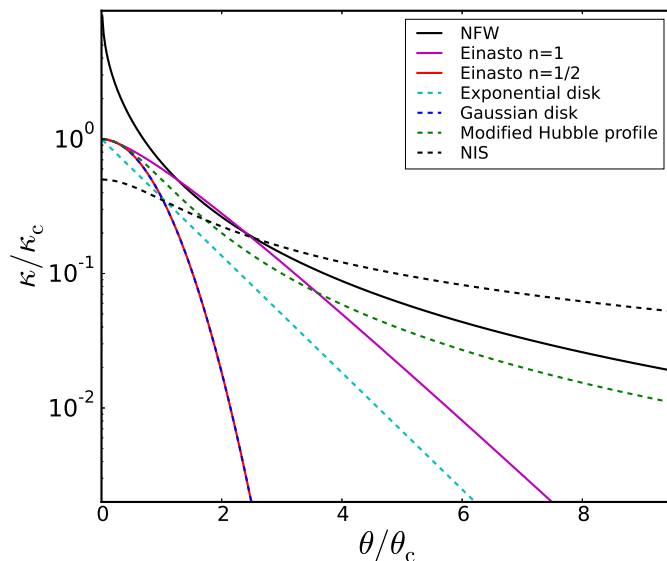


Fig. 6: Density profiles of the given lens models.

and modified Hubble model, the density profile decrease gradually at the outer part ( $\theta > 5\theta_c$ ) of the lens model. For the NIS model, its density profile decreases with a more gentle slope, and this lens model gives a higher magnification invariant, which equals 2. Thus in other words the slope of density profile can be a potential explanation for the different converged value of magnification invariants between the different lens models. Moreover, as indicated from the density profile, the total mass is convergence for the exponential disk lens and Einasto lens, but it is divergence for the lens with modified Hubble model and NFW lens. One of another potential explanation is the ratio of mass inside of the Einstein radius to the total mass,  $F = M(\leq \theta_E)/M_{\text{tot}}$ . We find that, for both exponential disk lens and Einasto lens ( $n = 1/2$  and 1), this mass ratio tends to 1 with the increasing of the characteristic surface mass density  $\kappa_c$ , while the mass ratio  $F \rightarrow 0$  for the modified Hubble profile and NFW lens. Combining with that  $F = 1$  for the point lens and  $F = 0$  for SIS and NIS, we speculate that when  $F \rightarrow 1$  of a given lens, it will act as a point lens and have a magnification invariant of  $I = 1$ . While a lens with  $F \rightarrow 0$ , for which the total mass is not converge, can hardly have a magnification invariant of  $I \rightarrow 1$  with the increasing of its model parameters. More detailed analyses in the future should be helpful to understand the contrast between these two different results.

#### 4 CONCLUSION AND DISCUSSION

Forming multiple images of the given background source is one of the most important effects of strong gravitational lensing. When the image number is a maximum, the summation of signed magnifications of the images can be a constant for certain lens models. For some quadruple lens models, it is found that the invariant is independent of most of the model parameters, as long as the source lies inside of the caustic (Dalal 1998). In this paper, we focus on several commonly used circular lens models, in which the magnification invariants have not been investigated before. We find that for the exponential disk lens model, magnification invariant should be existent, but with a very subtle change as changing of source position  $\beta$  in the caustic region. Moreover, we also calculate the magnifications of the other two important lens models, Gaussian

disk lens and modified Hubble profile lens. Our results indicate that magnification invariants do also exist for these two lens models.

Considering the dark matter halo can be described by some universal profiles, we further examine two typical models: singular two-parameter model, e.g. NFW lens, and non-singular three-parameter model, e.g. Einasto lens. With the thin lens approximation, we find that the magnification summations of three images for an arbitrary point source inside the caustic are constant for both the NFW and Einasto models .

More tests indicate that the magnification summation does not change with changing of the scale length  $\theta_c$ , because of that the lensing properties will not be changed if a dimensionless radial distance  $x = \theta/\theta_c$  is defined in the circular lens models. Thus the magnification invariants are independent of the characteristic radius  $\theta_c$ . However, the central density  $\kappa_c$  can affect the magnification summations significantly. In the paper, we show how the magnification summations of a given lens model vary as functions of the model parameters  $\kappa_c$  and  $\theta_c$ . When  $\kappa_c$  is very large, the magnification invariant tends to be 1 for both exponential disk lens and Einasto lens (both  $n = 1/2$  and 1), which can be explained as that the lens will act as a point mass with  $\kappa_c$  increasing. Moreover, the invariants of exponential disk lens and Einasto lens increase monotonically with the characteristic surface mass density  $\kappa_c$ , while it is decreasing for the modified Hubble profile and NFW lens. This difference should be resulted by the different density profiles of the lens models, and more detailed analyses should be helpful to understand the contrast between these two different results.

Observationally, combining the magnification invariants and the measurements of Type Ia supernovae (SNe Ia), which are excellent standard candles, we can constrain the lens model in more detail. While the invariant can be significantly affected by the substructure or high-order asymmetry of lens. In the future, the magnification of high-order lens model and of the haloes in  $N$ -body simulation or hydrodynamic simulation should be studied, and the magnification invariant can be examined in a more realistic manner.

**Acknowledgements** The authors thank Qianli Xia for helpful discussion and suggestions. We acknowledge the supports of the NSFC (No. 11403103, 11603032, 11333008, 11273061), the 973 program (No. 2015CB857003, 2013CB834900), China Postdoctoral Science Foundation (2014M551681) and the NSF of Jiangsu province (No. BK20140050).

## Appendix A: MAGNIFICATION INVARIANT FOR NIS

As an important lens model, the Singular Isothermal Sphere (SIS) has been widely used in the theoretical reserch. Another one more realistic model for modeling lensing galaxies is Non-singular Isothermal Sphere (NIS), which is profiled by isothermal sphere with a finite core  $\theta_c$ . In this case, by defining dimensionless radius  $x = \theta/\theta_c$ , the convergence of NIS is given by

$$\kappa_{\text{NIS}}(x) = \frac{\kappa_c}{2\sqrt{x^2 + 1}}, \quad (\text{A.1})$$

where  $\kappa_c$  is a constant for the given radial profile. Clearly, using 2D Poisson equation, the lensing functions can be derived as:

$$\alpha_{\text{NIS}}(x) = \frac{\kappa_c}{x} \left( \sqrt{x^2 + 1} - 1 \right), \quad (\text{A.2})$$

$$\gamma_{\text{NIS}}(x) = \frac{\kappa_c}{x^2} \left( \sqrt{x^2 + 1} - 1 \right) - \frac{\kappa_c}{2\sqrt{x^2 + 1}}. \quad (\text{A.3})$$

Then, for a given source position  $y_0$ , combining the lens equation  $y_0 = x - \alpha_{\text{NIS}}(x)$  and the magnification function  $1/\mu(x) = [1 - \kappa_{\text{NIS}}(x)]^2 - \gamma_{\text{NIS}}(x)^2$ , we can eliminate  $x$  to write a 3rd-degree polynomial equations about  $\mu$  as

$$A\mu^3 + B\mu^2 + C\mu + D = 0. \quad (\text{A.4})$$

Here the four coefficients related to the source position  $y_0$  and the model parameter  $\kappa_c$  are,

$$\begin{cases} A = y_0^2 [y_0^4 - y_0^2(2\kappa_c^2 + 10\kappa_c - 1) + \kappa_c(\kappa_c - 2)^3], \\ B = -2y_0^2 [y_0^4 - y_0^2(2\kappa_c^2 + 10\kappa_c - 1) + \kappa_c(\kappa_c - 2)^3], \\ C = y_0^6 - y_0^4(3\kappa_c^2 + 10\kappa_c - 1) + y_0^2\kappa_c(3\kappa_c^3 + 4\kappa_c^2 \\ \quad + 8\kappa_c - 8) - \kappa_c^2(\kappa_c^2 - 3\kappa_c + 2)^2, \\ D = 4\kappa_c^2 [y_0^2 + (\kappa_c - 1)^2]. \end{cases}$$

Thus, we can obtain three roots at most, and these three magnifications  $(\mu_1, \mu_2, \mu_3)$  correspond to the three images of source at  $y_0$  for the given NIS parameter  $\kappa_c$ . As described by the Vieta's formulas in mathematics, we are able to calculate the sum of these magnifications by

$$\sum_{i=1}^3 \mu_i = -\frac{B}{A} = 2. \quad (\text{A.5})$$

Therefore, one can rigidly prove that the magnification invariant is  $I = \sum_i \mu_i = 2$  for the NIS lens model, providing the source is inside the caustic. Moreover, this invariant is independent of the parameters  $y_0$  and  $\kappa_c$ .

## References

- Aazami, A. B., & Petters, A. O. 2009, *Journal of Mathematical Physics*, 50, 032501
- Aubert, D., Amara, A., & Metcalf, R. B. 2007, *MNRAS*, 376, 113
- Bartelmann, M. 1996, *A&A*, 313, 697
- Biggs, A. D., Browne, I. W. A., Helbig, P., et al. 1999, *MNRAS*, 304, 349
- Binney, J., & Tremaine, S. 1987, Princeton, NJ, Princeton University Press, 1987
- Burke, W. L. 1981, *ApJ*, 244, L1
- Cao, S., Biesiada, M., Gavazzi, R., Piórkowska, A., & Zhu, Z.-H. 2015, *ApJ*, 806, 185
- Chu, Z., Li, G. L., & Lin, W. P. 2015, *MNRAS*, 449, 2079
- Chu, Z., Li, G. L., Lin, W. P., & Pan, H. X. 2016, *MNRAS*, 461, 4466
- Dalal, N. 1998, *ApJ*, 509, L13
- Dalal, N., & Rabin, J. M. 2001, *Journal of Mathematical Physics*, 42, 1818
- Dhar, B. K., & Williams, L. L. R. 2010, *MNRAS*, 405, 340
- Dyer, C. C., & Roeder, R. C. 1980, *ApJ*, 238, L67
- Elíasdóttir, Á., & Möller, O. 2007, *J. Cosmol. Astropart. Phys.*, 7, 006
- Fassnacht, C. D., Xanthopoulos, E., Koopmans, L. V. E., & Rusin, D. 2002, *ApJ*, 581, 823
- Golse, G., & Kneib, J.-P. 2002, *A&A*, 390, 821

- Hurtado, R., Castañeda, L., & Tejeiro, J. M. 2014, *International Journal of Astronomy and Astrophysics*, 4, 340
- Koopmans, L. V. E., Bolton, A., Treu, T., et al. 2009, *ApJ*, 703, L51
- Kormann, R., Schneider, P., & Bartelmann, M. 1994, *A&A*, 284, 285
- Lehár, J., Falco, E. E., Kochanek, C. S., et al. 2000, *ApJ*, 536, 584
- Linder, E. V. 2011, *Phys. Rev. D*, 84, 123529
- Mao, S., Witt, H. J., & Koopmans, L. V. E. 2001, *MNRAS*, 323, 301
- McKean, J., Jackson, N., Vegetti, S., et al. 2015, *Advancing Astrophysics with the Square Kilometre Array (ASKA14)*, 84
- Meylan, G., Jetzer, P., North, P., et al. 2006, *Saas-Fee Advanced Course 33: Gravitational Lensing: Strong, Weak and Micro* (Berlin: Springer)
- Miralda-Escude, J. 1991, *ApJ*, 370, 1
- Narayan, R., & Bartelmann, M. 1999, *Formation of Structure in the Universe*, 360
- Navarro, J. F., Hayashi, E., Power, C., et al. 2004, *MNRAS*, 349, 1039
- Navarro, J. F., Frenk, C. S., & White, S. D. M. 1997, *ApJ*, 490, 493
- Navarro, J. F., Ludlow, A., Springel, V., et al. 2010, *MNRAS*, 402, 21
- Paraficz, D. 2009, Ph.D. Thesis
- Petters, A. O., & Werner, M. C. 2010, *General Relativity and Gravitation*, 42, 2011
- Retana-Montenegro, E., & Frutos-Alfaro, F. 2011, arXiv:1108.4905
- Retana-Montenegro, E., Frutos-Alfaro, F., & Baes, M. 2012, *A&A*, 546, A32
- Retana-Montenegro, E., van Hese, E., Gentile, G., Baes, M., & Frutos-Alfaro, F. 2012, *A&A*, 540, A70
- Rood, H. J., Page, T. L., Kintner, E. C., & King, I. R. 1972, *ApJ*, 175, 627
- Rusin, D., Keeton, C. R., & Winn, J. N. 2005, *ApJ*, 627, L93
- Schneider, P., Ehlers, J., & Falco, E. E. 1992, *Gravitational Lenses, XIV*, (Berlin: Springer), 112
- Sereno, M., Fedeli, C., & Moscardini, L. 2016, *J. Cosmol. Astropart. Phys.*, 1, 042
- Shu, Y., Bolton, A. S., Mao, S., et al. 2016, *ApJ*, 833, 264
- Shu, Y., Brownstein, J. R., Bolton, A. S., et al. 2017, *ApJ*, 851, 48
- Suyu, S. H., Treu, T., Hilbert, S., et al. 2014, *ApJ*, 788, L35
- Tortora, C. 2007, *1st Workshop of Astronomy and Astrophysics for Students*, 127
- Trotter, C. S., Winn, J. N., & Hewitt, J. N. 2000, *ApJ*, 535, 671
- Tsukamoto, N., & Harada, T. 2013, *Phys. Rev. D*, 87, 024024
- Vegetti, S., Lagattuta, D. J., McKean, J. P., et al. 2012, *Nature*, 481, 341
- Werner, M. C. 2009, *Journal of Mathematical Physics*, 50, 082504
- Witt, H. J., & Mao, S. 2000, *MNRAS*, 311, 689
- Wright, C. O., & Brainerd, T. G. 2000, *ApJ*, 534, 34
- Yuan, C. C., & Wang, F. Y. 2015, *MNRAS*, 452, 2423